Bull. Chem. Soc. Ethiop. **2022**, 36(3), 531-544.
DOI: https://dx.doi.org/10.4314/bcse.v36i3.4

ISSN 1011-3924
Printed in Ethiopia
Online ISSN 1726-801X

EFFICIENT REMOVAL OF METHYL ORANGE USING MAGNESIUM OXIDE NANOPARTICLES LOADED ONTO ACTIVATED CARBON

M. Venkata Ratnam[1*], Meena Vangalapati[2], K. Nagamalleswara Rao[3] and K. Ramesh Chandra[4]

[1]Department of Chemical Engineering, Mettu University, Mettu, Ethiopia
[2]Department of Chemical Engineering, A.U. College of Engineering, Vizag, Andhra Pradesh, India
[3]School of Chemical Engineering, Vellore Institute of Technology, Vellore, Tamil Nadu, India
[4]Department of Chemical Engineering, RVR & JC College of Engineering, Guntur, Andhra Pradesh, India

Received December 7, 2021; Revised June 20, 2022; Accepted June 20, 2022

ABSTRACT. In this work, an activated carbon composite made with magnesium oxide nanoparticles (MgONP-AC) was effectively utilized for methyl orange (MO) adsorption. The effect of pH (6-10), mass of MgONP-AC (0.1-0.3 g/L), initial MO concentration (10-30 mg/L), and temperature (283-323 K) on MO removal was investigated using a central rotatable composite experimental design based on the response surface technique (RSM) at an equilibrium agitation period of 60 min. The studies predicted the optimal MO removal of 98.99% at pH 7.68, MgONP-AC dosage of 0.24 g/L, and starting MO concentration of 15 mg/L, and temperature of 313 K. Furthermore, an artificial neural network (ANN) was utilized to simulate MO adsorption, and it properly predicted MO removal using mean squared error (MSE) and R^2 for the testing data. The ANN predicts a maximum removal of 99.63% with ANN with $R^2 = 0.9926$. The kinetic results suited the pseudo-second order kinetic equation, and the data from the equilibrium investigations corresponded well with the Langmuir isotherm (maximum uptake capacity q_{max} = 346 mg/g). Endothermic, spontaneous, and physical adsorption were discovered during the thermodynamic investigations.

KEY WORDS: Adsorption, Artificial neural network, Experimental design, isotherms, Kinetics, Methyl orange, MgONP-AC

INTRODUCTION

Industrialization has been linked to environmental degradation as a result of toxic and harmful industrial effluents [1]. To limit pollution and restore ecosystems, strict restrictions have been imposed all over the world [2]. Industrial water usage has expanded considerably (approximately 20% of available freshwater), resulting in massive amounts of effluent containing significant contaminants [3–6]. Because synthetic dyes are a major source of water pollution, the growth of the textile and dyeing industries causes considerable environmental issues [7]. Almost 10% of the seven lakh tons of dyes produced globally each year are commonly combined with water bodies, causing a variety of environmental issues. The fundamental difficulty with dyes is that they are not only toxic and carcinogenic, but they also hinder the photosynthetic cycle, producing issues in the aquatic system even in little amounts [8]. Dyes, which are organic molecules in nature, are resistant to biodegradation and produce hazardous by-products as a result of incomplete breakdown. Dyes are the most difficult and time-consuming contaminants to remove using traditional procedures due to their structural complexity [9, 10].

Because it is simple and effective, adsorption is undoubtedly the most explored color treatment method [11–14]. Activated carbon is a significant adsorbent due to its porous character, higher surface area, excellent acid/basic stability, and presence of functional groups such as –OH [15]. Because of the higher initial cost and complexity of regeneration, activated carbon is a less

*Corresponding author. E-mail: mvratnam81@gmail.com

practicable adsorbent, highlighting the significance of alternative, efficient adsorbents. There has been a lot of interest in nanoscale metal oxides as improved environmental and energy materials in recent years [16]. Because of their small size, high porosity, and active surface, metal oxide nanoparticles have substantial pollutant-binding capacities as compared to bulk materials [17, 18]. They can even be chemically replenished after being depleted. These particles have distinct features such as higher catalytic potential and strong reactivity, making them more efficient adsorbing materials than standard ones. The development of environmentally friendly adsorbents is becoming a key issue in pollution control. There is a considerable body of research on the effective use of metal oxide nanoparticles for hazardous pollutant removal, such as iron oxides, zinc, calcium, magnesium, aluminum, and titanium [12, 17–22].

Magnesium oxide is a low-cost, high-potential alkaline metal oxide. It has a high surface activity and is a damaging sorbent. However, the stability of MgO nanoparticles is still an important factor that will influence the material's qualities. Material pairings alter functional groups, resulting in better properties. A variety of metallic/bimetallic nanoparticles were formed on activated carbon and their dye adsorption capabilities were investigated [23–27]. The more reactive centers there are in hybrid nanocomposite materials, the greater their performance [27]. Several investigations in the literature suggest that carbon-supported MgO nanoparticles may be used for a range of applications, including transesterification catalysts [28], CO_2 capture adsorbents [29], acetone capture [30], H_2S removal [31], and antibacterial agents [32–34]. Printing, textiles, paper, medicines, and food processing all employ methyl orange (MO). MO causes liver damage, lung inflammation, brain trauma, central nervous system damage, and reproductive system dysfunction in humans.

The destructive nature of magnesium oxide coupled with functional groups of activated carbon makes a brilliant adsorbent for handling toxic pollutants. In this work, magnesium oxide (MgONP) nanoparticles were coated on an activated carbon surface (MgONP-AC) for adsorption of the MO dye. The adsorbent was studied using X-ray diffraction (XRD), scanning electron microscopy (SEM), and Fourier transformation infrared spectroscopy (FTIR). To forecast and improve the adsorption process, response surface methodology (RSM) based on central composite (CCD) and MATLAB artificial neural networks (ANN) were utilized. To further understand the adsorption mechanism, kinetic, equilibrium, and thermodynamic experiments were carried out.

EXPERIMENTAL

Chemicals

All the required chemicals were procured and used without any purification. Merck Chemicals supplied magnesium nitrate GR ($Mg(NO_3)_2.6H_2O$). Polyvinylpyrrolidone (PVP) and ammonium hydroxide (NH_4OH) were procured from LobaChemie Pvt. Ltd. (India). Activated carbon and ethanol was procured from Fisher Scientific. The stock solution of 1000 mg/L of MO dye (molecular formula: $C_{14}H_{14}N_3NaO_3S$, molecular weight: 327.34 g/mol, Merck) is prepared by dissolving 1 g of dye in de-ionized water. Dye solutions of various concentrations were obtained by dilution. The pH was adjusted using solutions of hydrochloric acid (0.1 N) and sodium hydroxide (0.1 N).

MgONP-AC synthesis and characterization

The chemical precipitation technique was used to make nano-MgO, which was then calcined at 500 °C with magnesium nitrate hexahydrate ($Mg(NO_3)_2.6H_2O$) as a precursor metal, poly vinyl pyrrolidone (PVP) as a stabilizer, and ammonium hydroxide (NH_4OH) as a precipitating agent. The detailed procedure is explained in our earlier studies [32, 33]. The hybrid adsorbent was created by dispersing 1 g of MgO nanoparticles in ethanol with 5 g of activated carbon. To

guarantee uniform loading of MgO nanoparticles on the activated carbon surface, the mixture is continuously stirred for 12 h at 300 rpm speed and room temperature. To eliminate the ethanol contained in the precipitate, it was filtered and heated to 80 ºC. After that, the residue was rinsed several times with de-ionized water and dried at room temperature. MgONP-AC was the name given to the produced composite, which was analyzed using a Regaku X-ray diffractometer with Cu-Kα radiation (λ = 1.5418 Å, scan rate: $0.05^{o}s^{-1}$, 2θ range: 100-800) and field emission scanning electron microscopy (FE-SEM Carl Zeiss NTS GmbH, Germany). The functional groups responsible for adsorption were evaluated using the Fourier Transmission Infrared (FT-IR) spectrum.

Adsorption experiments

In batch mode, the following adsorption experiment was carried out: At room temperature, 50 mL of MO solution with a significant concentration and pH was treated with the necessary quantity of MgONP-AC for a predetermined time period. A centrifuge was used to separate the adsorbent, and a UV-Spectrophotometer was used to determine the residual dye concentration. The % MO eliminated was calculated using the formula:

$$\%\ \text{MO removal} = (C_o - C_t)/C_0 \times 100 \quad (1)$$

where C_o (mg/L) and C_t (mg/L) are the initial and final concentrations of MO sample at time t=0, respectively. The MO adsorbed on the MgONP-AC surface was estimated using the equation:

$$q_e = (C_o - C_e)V/W \quad (2)$$

where C_o and C_e (mg/L) are initial and equilibrium MO concentrations in aqueous solution, respectively, W (g) is the mass of MgONP-AC and the volume of the solution is V(L).

Computing the R-square (R^2) for the non-linear approach is advised in addition to calculating the chi-squared value (χ^2) to select the best kinetic, isotherm model that matches the experimental data. If the model's output is identical to the experimental output, the chi-square value will be zero, and vice versa. As a result, large values of R^2 and low values of $\chi^2$are required for a model to properly match experimental data. The following formulae are used to determine the values of χ^2 and R^2.

$$\chi^2 = \sum \frac{(q_{e,exp} - q_{e,cal})^2}{q_{e,cal}} \quad (3)$$

$$R^2 = 1 - \frac{\sum(q_{e,exp} - q_{e,cal})^2}{\sum(q_{e,exp} - q_{e,mean})^2} \quad (4)$$

where $q_{e,exp}$ and $q_{e,cal}$ are the experimental and calculated uptake capacities, respectively.

Experimental design-response surface methodology

All experimental runs were performed under the conditions indicated by RSM, which was based on CCD. By fitting the experimental data into a polynomial equation with probable interactions between the experimental variables, the RSM was utilized to determine the optimum experimental circumstances. The CCD has 3 sets of experimental runs: (1) factorial runs in which factors are investigated, (2) center points, and (3) axial points in which the design can be rotated. The experimental error and data reproducibility are calculated using the center points. The axial points are located at (±α, 0, 0), (0, ±α, 0) and (0, 0, ±α), where α is the axial point distance from center. In this study, α value was fixed at 2.The independent variables selected for optimization were X_1, pH; X_2, MgONP-AC dosage; X_3, MO concentration and X_4, Temperature. The quadratic

regression model, which can be stated as follows (Eq.5), is the most commonly used model for explaining the connection between essential input elements and quantifiable output.

$$y = \beta_0 + \sum_{i=1}^{k} \beta_i x_i + \sum_{i=1}^{k} \beta_{ii} x_i^2 + \sum_{i,j\geq 1}^{k} \beta_{ij} x_i x_j + \varepsilon \quad (5)$$

where x is input variable and y is the process response; k is the number of factors; i and j are index numbers for factors; β_0 is the offset term; β_i is the coefficient of first-order effect (i.e., linear, primary effect); β_{ii} is the quadratic effect (i.e. squared effect); β_{ij} represents the interaction, and ε is the error between predicted and observed values.

Artificial neural networks (ANN) for modeling

In this work, a three-layer feed-forward ANN comprising an input layer, a hidden layer, and an output layer was created for modeling. The input layers were pH, dose, concentration, and temperature, with the output layer being percent MO adsorbed. To determine which back-propagation (BP) approach has the lowest mean squared error (MSE), the mean squared error (MSE) and relative error (RE) were computed. The most successful approach for training the network was demonstrated to be the Levenberg–Marquardt back propagation method (LMA). Using the ANN tool box in MATLAB 2021a, all experimental data (30 runs) was randomly split into three groups: 70% for training, 15% for cross validation, and 15% for assessing the accuracy of the model and prediction. To decrease network error, the input variables and response were normalized between 0 and 1. The optimal number of neurons in the hidden layer was established by trial and error using a range of topologies in order to obtain the lowest mean square error (MSE) and highest correlation coefficient (R^2) [35–37]. This was done to ensure that forecasts differed as little as possible from experimental data, as well as to prevent the possibility of over-fitting the model [38–40]. Large and small numbers of neurons were avoided since they might lead to complicated over fitting and a decrease in convergence rate, respectively.

RESULTS AND DISCUSSION

Characterization of the adsorbent

Figure 1(a) and 1(b) illustrate the surface morphology of MgONP and MgONP-AC as investigated by FE-SEM. The cubic form of MgONP is depicted in Figure 1(a), while the dispersion of MgONP over the surface of activated carbon is depicted in Figure 1(b). Figure 1(c) shows the XRD pattern of the synthesized nanocomposite, MgONP-AC. The lattice planes of MgO (1 1 1), (2 0 2), and (3 1 1) cubic structures are shown by peaks at 38°, 62°, and 74°. The results show that the crystalline shape of MgONP was retained after compositing with activated carbon. Figure 1 (d) depicts the FTIR spectra for untreated and MB-treated adsorbents with wave numbers ranging from 400 to 4000 cm^{-1}. The existence of nano-sized MgO is verified by the appearance of significant peaks between 660 and 540 cm^{-1} [41, 42]. The stretching vibrations correspond to magnesium oxide and were observed at around 860 and 600 cm^{-1} [43]. Because magnesium nitrate was used as the precursor, the signal at 869 cm^{-1} reveals the observable presence of MgO as well as (O-C=O). The distinctive band at 3697 cm^{-1} for unused MgONP-AC can be attributed to O–H bending vibrations [44, 45]. The C-C vibrations exhibit a band at 1400–1450 cm^{-1}.

The narrow peak seen following MB adsorption at 1020 cm^{-1} corresponds to C–O stretching. The stretching frequency of 2954–2835 cm^{-1} was connected to vibrations of the C–H bond. The FTIR study of methyl orange treated adsorbent MgONP-AC in comparison to unused adsorbent reveals broader peak positions at 3697, 2949, and 2881cm^{-1}, indicating that the adsorbent containing functional groups was physically bound with methyl orange dye and dye adsorption was effective on the adsorbent's surface. The additional peaks found between 1000-1500 cm^{-1}

after adsorption corresponded to the C–N, >C=O, and C–S functions. The adsorption appears to be the result of π-π stacking interactions between the aromatic backbone of the methyl orange dye and the skeleton of activated carbon.

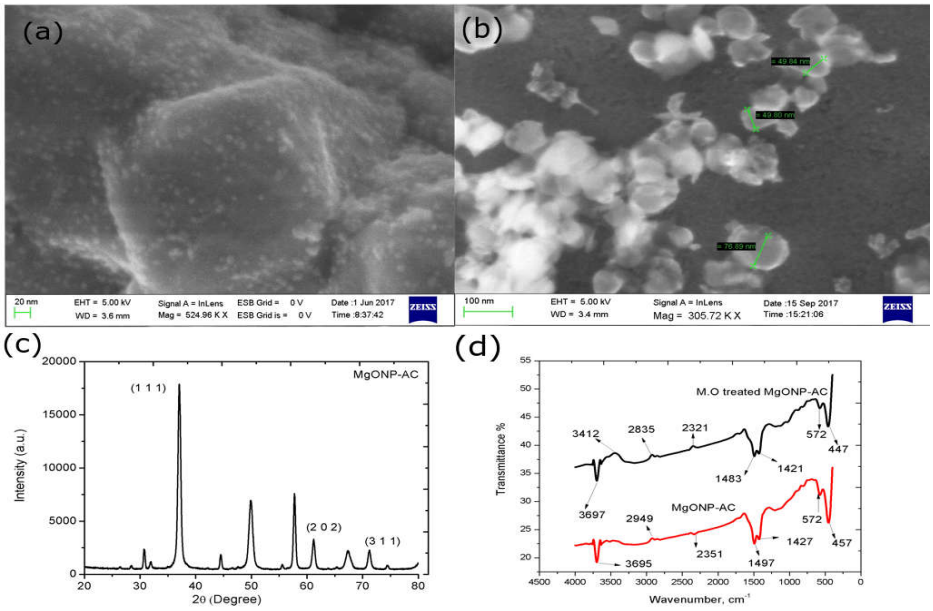

Figure 1. (a): SEM image of MgONP; (b): SEM image of MgONP-AC; (c): XRD diagram of MgONP-AC; (d): FTIR images of unused and MO treated MgONP-AC.

RSM-based experimental design and optimization

The percent adsorption of MO by MgONP-AC was investigated at various agitation periods for samples with 20 mg/L MO concentration, 0.2 g/L adsorbent dose at pH 5.5 and 303 K temperature. The adsorption rate of MO was found to be fast in the early stages, and the equilibrium period was found to be 60 min with 92.15% MO adsorption. As a result, further tests were conducted at 60 min agitation time. A four-factor CCD (central composite design) based on 30 experimental runs at various numerical values of pH (X_1), adsorbent dosage (X_2), initial dye concentration (X_3), and temperature (X_4) was conducted to investigate their main and interaction contribution to recovery of dyes while keeping agitation time for methyl orange constant at its equilibrium value i.e. 60 min. Table 1 presents the results of CCD studies and the ANOVA results are given in Table 2.

ANOVA (analysis of variance)

The low probability (0.05) and F-value of 535.8 showed that the model was accurate. Furthermore, the acceptable and reasonable value of lack of fit with F-value of 0.2377 with probability (>0.05) was a strong indicator of the method's suitability for outstanding experimental data presentation. The model has a significant R^2 value of 0.9970 for MO removal, suggesting that the experimental and predicted results are in good agreement. Furthermore, the anticipated R^2 value of 0.9908 corresponded to the modified R^2 value of 0.9951.The adequate precision (signal

to noise ratio) of the model was 102.491, demonstrating that this model can be utilized to traverse the design space.

Table 1. Results from CCD for MO adsorption onto MgONP-AC.

Run no.	X_1, pH	X_2, w	X_3, C_0	X_4, T	% adsorption of MO	
					Experimental	Predicted
1	9.00	0.15	25.00	313.00	87.77	87.35
2	9.00	0.15	15.00	293.00	86.94	86.47
3	9.00	0.25	15.00	293.00	89.58	89.60
4	9.00	0.25	25.00	293.00	86.58	87.10
5	9.00	0.15	15.00	313.00	89.3	89.85
6	7.00	0.15	15.00	293.00	90.5	90.47
7	9.00	0.15	25.00	293.00	83.98	83.97
8	8.00	0.20	20.00	303.00	95.95	95.83
9	9.00	0.25	25.00	313.00	90.55	90.48
10	8.00	0.20	20.00	323.00	98.24	98.46
11	7.00	0.25	15.00	293.00	92.65	92.78
12	8.00	0.20	20.00	283.00	90.83	90.59
13	7.00	0.25	25.00	313.00	96.29	96.31
14	8.00	0.10	20.00	303.00	89.65	89.83
15	10.00	0.20	20.00	303.00	77.19	77.37
16	9.00	0.25	15.00	313.00	93.43	92.98
17	8.00	0.20	20.00	303.00	96	95.83
18	7.00	0.15	15.00	313.00	95.02	94.96
19	7.00	0.15	25.00	293.00	89.41	89.49
20	7.00	0.25	25.00	293.00	91.55	91.81
21	8.00	0.20	20.00	303.00	95.43	95.83
22	8.00	0.20	20.00	303.00	96.12	95.83
23	8.00	0.20	30.00	303.00	92.82	92.63
24	7.00	0.15	25.00	313.00	93.96	93.99
25	8.00	0.20	20.00	303.00	95.67	95.83
26	8.00	0.20	10.00	303.00	95.93	96.10
27	8.00	0.30	20.00	303.00	95.47	95.27
28	8.00	0.20	20.00	303.00	95.8	95.83
29	7.00	0.25	15.00	313.00	97.3	97.28
30	6.00	0.20	20.00	303.00	87.39	87.19

Response surface plots and interactions between the adsorption parameters for MO adsorption using MgONP-AC

Figure 2(a)–2(c) show response surface contour plots of the percent adsorption of MO vs. the interaction effects of pH, initial MO concentration, adsorbent dose, and aqueous solution temperature. These plots were created for a specific pair of components at defined and optimum values of other variables. The curvatures of these graphs represent the interplay of the factors. The relationship of pH and adsorbent dose for MO removal is seen in Figure 2 (a). Because of the large surface area accessible, the MO removal has increased with usage of increased adsorbent. At the same time, changes in solution pH have a significant impact on the percent removal, confirming that electrostatic interactions are the major cause of MO adsorption. The interaction impact of initial MO concentration and aqueous solution pH on MO adsorption is seen in Figure 2(b). The availability of a greater number of active sites is clearly supported by maximum adsorption at lower MO concentrations. The removal of MO fluctuated drastically with pH, indicating that the adsorbent surface was extremely pH sensitive. The interplay of pH and

temperature is seen in Figure 2(c). The three-dimensional figure demonstrates the favorable relationship between temperature and MO elimination %.

Table 2. ANOVA Table for model to predict % removal of MO by MgONP-AC using CCD.

Source	Sum of squares	*Df*	Mean square	*F* Value	*p*-value
Model	624.20	11	56.75	535.80	< 0.0001
X_1-*pH*	144.80	1	144.80	1367.19	< 0.0001
X_2-dosage	44.53	1	44.53	420.43	< 0.0001
X_3-Conc.	18.11	1	18.11	171.03	< 0.0001
X_4-Temp	93.02	1	93.02	878.34	< 0.0001
X_1X_2	0.66	1	0.66	6.23	0.0225
X_1X_3	2.33	1	2.33	22.03	0.0002
X_1X_4	1.26	1	1.26	11.90	0.0029
X_1^2	314.65	1	314.65	2970.98	< 0.0001
X_2^2	18.42	1	18.42	173.92	< 0.0001
X_3^2	3.67	1	3.67	34.64	< 0.0001
X_4^2	2.91	1	2.91	27.48	< 0.0001
Residual	1.91	18	0.11		
Lack of Fit	1.59	13	0.12	1.95	0.2377
Pure Error	0.31	5	0.063		
Cor Total	626.11	29			

df - degree of freedom; SS - sum of squares; F - factor F; P – probability.

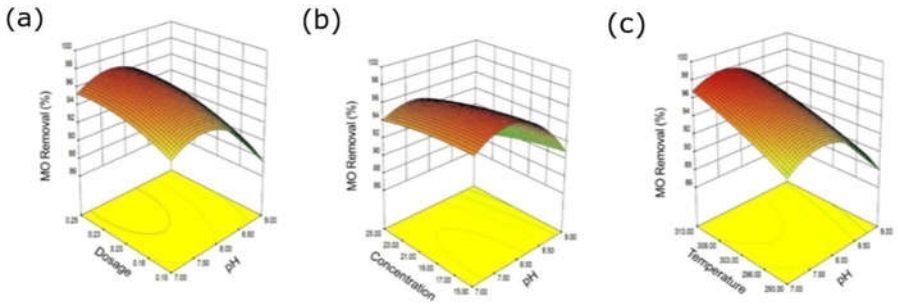

Figure 2. (a), 2(b), 2(c): 3D response surface plots for adsorption of MO onto MgONP-AC interactive effects of pH and dosage; pH and concentration; pH and temperature.

Optimization

By evaluating the percent removal to be maximized, the optimal circumstances are determined to be a pH of 7.68, a dose of 0.24 g/L, and an initial MO concentration of 15 mg/L at a temperature of 313 K. The elimination rate was 98.89%, with an overall desirability of 0.952. The experimental removal % at the optimum process variables was carried out, and it agrees well with the theoretical value obtained from the desirability analysis.

Modeling by artificial neural networks

The Levenberg-Marquardt (LM) back propagation approach was used to train the ANN network, which is one of the Multi-Layer Perception (MLP) networks used for error reduction. Throughout the training period, different numbers of neurons ranging from 1 to 10 were tested. The ANN

model's success is assessed by maximizing the R^2 value and reducing the MSE of the training set. An ANN with five hidden neurons predicted adsorption behavior the best. As a consequence, 4-5-1 is the best design of the neural network (four input neurons indicating pH, dose, starting concentration, and temperature; five hidden neurons in a single layer; and one output neuron representing the percentage elimination). The training was terminated after 6 epochs. The ANN regression illustrates the experimental network target information and normalized projected outputs for training, validation, testing, and total data. The correlations for training, testing, validation, and total data were 0.999, 0.9761, 0.9766, and 0.9926, respectively. The ANN's significant correlation and prediction precision is owing to its well-known ability to mimic the system's nonlinearity.

A linear regression study comparing experimental and ANN-predicted color removal was undertaken to evaluate network performance, with the linear regression coefficient (R^2) for both ANN-predicted and experimental color removal being close to one. This implies that the trained ANN model's forecast was correct. Under a temperature of 313 K, the color removal achieved utilizing the ANN method was 99.63% at optimal circumstances of pH 7.68, dosage 0.24 g/L, and an initial MO concentration of 15 mg/L. Figure 3 (a), (b) presents the correlation plots for RSM, ANN predicted values with experimental values, respectively. The comparison of both RSM and ANN models reveals that ANN was better, although both achieved comparable outcomes.

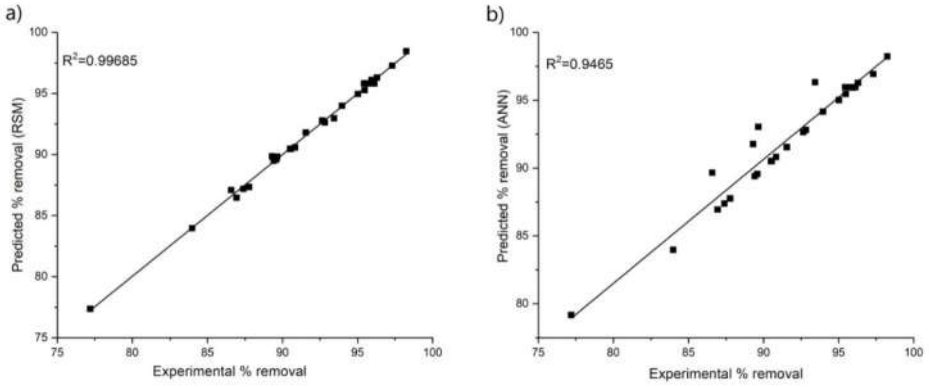

Figure 3. Correlation plot of experimental data with (a) RSM predicted values and (b) ANN predicted values.

Kinetic studies

The non-linear regression of experimental kinetics is plotted using all four kinetic models, Pseudo-first order, Pseudo-second order, Elovich, and Intra-particle diffusion. Table 3 shows the experimental data that was associated with the four models, the model parameters and constants for each model. The considerable disparity in predicted and experimental q_e values, along with the low value for R^2 (0.9573), indicate that the pseudo-first order kinetics model is unsuitable for describing the experimental data. The applicability of Pseudo-second order kinetics for interpretation of experimental data of MO adsorption by MgONP-AC adsorbent was evident from high R^2 values and low χ^2 values. MO adsorption onto MgONP-AC typically exhibits a relatively good coefficient of linear regression (R^2 = 0.9936) for the elovich model with an initial rate constant (α) of 13.2 mg/g.min and a low desorption rate constant (β = 0.104 g/mg). To decide on the actual rate controlling step involved in the MO adsorption onto MgONP-AC, intra-particle diffusion model was employed. For the intra-particle diffusion model, the values of q_t were found

to be multi-linearly correlated with values of $t^{1/2}$. The initial adsorption factor of $R_i = [1–(C/q_{ref})]$ of 0.8154, which is in between 0.5 and 0.9 indicates that the process is intermediately initial adsorption, and the boundary layer thickness was 7.426 mg/g. K_{diff}, the rate constant for intra-particle diffusion, was obtained as 5.127 mg/g.min$^{1/2}$.

Table 3. Kinetic parameters and their correlation coefficients calculated for the adsorption of MO onto MgONP-AC (pH = 8; dosage = 0.2 g.L^{-1}; concentration = 20 mg.L^{-1}; temperature = 303 K).

Model	Parameters	Units		Values
Pseudo-first order $q_t = q_e(1 - e^{-k_1 t})$	k_1	(min^{-1})		0.123
	q_e (calc)	mg.g^{-1}		37.54
	R^2			0.9573
	χ^2			2.92
Pseudo-second order $q_t = \frac{q_e^2 k_2 t}{1 + q_e k_2 t}$	k_2	(g.mg^{-1}min^{-1})		0.0035
	q_e (calc)	mg.g^{-1}		43.95
	R^2			0.9891
	χ^2			0.528
Elovich $q_t = \frac{\ln(1 + \alpha\beta t)}{\beta}$	β	(g.mg^{-1})		0.104
	α	(mg.g^{-1}.min^{-1})		13.2
	R^2			0.9936
	χ^2			0.2858
Intra-particle diffusion $q_t = k_{diff} t^{0.5} + C$	K_{diff}	(mg.g^{-1}.min$^{-1/2}$)		5.127
	C	(mg.g^{-1})		7.426
	R_i			0.8154
	R^2			0.92
	χ^2			3.572
	q_e (Exp.)	mg.g^{-1}		42.15

Equilibrium studies

The key to understanding the adsorption process remains equilibrium information. By fitting the experimental data to non-linear equation forms of the isotherms, the applicability of standard models such as Langmuir, Freundlich, Temkin, and Redlich-Peterson isotherms was evaluated and assessed. The three-parameter isotherm, i.e. the R-P isotherm, was better fitted with non-linear regression than with trial and error based linear regression, and 'g', the R-P constant, was close to unity (0.97), indicating that the R-P isotherm was nearing the Langmuir isotherm. Table 4 lists the isotherm constants, the correlation coefficients (R^2, χ^2). High values of R^2 and low-values of χ^2 for Langmuir isotherm suggested that equilibrium would be best explained by Langmuir isotherm. The highest adsorption capacity for MO removal was obtained at 345.91 mg/g. Depending on the separation factor $R_L = \frac{1}{1+K_L C_O}$, the adsorption could be evaluated as irreversible (R_L= 0), favorable (0<R_L< 1), linear (R_L = 1) and unfavorable (R_L> 1).Similarly, a value in the range of 0 to 1 for the Freundlich constant 'n' indicates favorable adsorption. The R_L value was in the 0.0094-0.222 range, while the value of 'n' was obtained to be 0.2452 strongly supporting the favorable adsorption. The adsorbent–adsorbate interactions are taken into consideration in the case of the Temkin isotherm. The equilibrium data fitted with the Temkin model gives the heat of sorption (b) of 41.9 J.mol^{-1} calculated from the Temkin constant (B = RT/b) and the equilibrium binding constant (K_T) obtained as 6.198 L.mg^{-1}. The results show that adsorbent-adsorbate interactions minimize adsorption heat while improving coverage. As a result, dye adsorption was distinguished by a constant range of binding energies up to and including the maximum value.

Table 4. Isotherm constants and their correlation coefficients calculated for the adsorption of MO onto MgONP-AC (Agitation time = 60 min, pH = 8; dosage = 0.2 $g.L^{-1}$; temperature = 303 K).

Model	Parameters		Values
Langmuir $q_e = \frac{q_{max} k_L C_e}{(1 + k_L C_e)}$	q_{max}	$(mg.g^{-1})$	345.91
	k_L	$(L.mg^{-1})$	0.3504
	R_L		0.0094-0.222
	R^2		0.9923
	χ^2		6.3316
Freundlich $q_e = K_F C_e^n$	n		0.2452
	K_F	$(mg.g^{-1})/(mg.L^{-1})^n$	132.65
	R^2		0.878
	χ^2		66.295
Temkin $q_e = B \ln(C_e K_T)$	B		60.1125
	K_T	$(L.mg^{-1})$	6.198
	R^2		0.9694
	χ^2		12.377
Redlich-Peterson (R-P) $q_e = \frac{k_{rp} C_e}{(1 + a_{rp} C_e^g)}$	k_{rp}	$(L.g^{-1})$	134.273
	a_{rp}	$(mg.L^{-1})^{-g}$	0.4336
	g		0.9701
	R^2		0.9935
	χ^2		4.5719

Thermodynamics

Both energy and entropy must be considered in environmental applications, in order to determine the spontaneous nature of processes. The van't Hoffs thermodynamic analysis (Table 5) for MO adsorption was spontaneous (negative Gibbs free energy, ΔG°) and endothermic (positive enthalpy change, ΔH°), with randomness of the solid-liquid interface during the reaction (entropy, ΔS°).

Table 5. Thermodynamic parameters for adsorption of MO by MgONP-AC.

Temperature (K)	Equilibrium constant K_C	ΔG° (K.J/mol)	ΔH° (J/mol.K)	ΔS° (J/mol.K)	Van't Hoff equation
298	2.635	-2.4005	10.852	44.937	lnKc = -1305.35/T+5.405
303	3.143	-2.8849			
308	3.29	-3.0495			
313	3.476	-3.2421			
318	3.64	-3.4158			
323	3.826	-3.6034			

Mechanism of adsorption

Adsorption is primarily influenced by MgONP's high surface activity and the presence of -OH functional groups. The π-π stacking interaction between the aromatic backbone of the methyl orange dye and activated carbon may have aided adsorption. The adsorption of MO by MgONP-AC appears to be more pH sensitive. Adsorption experiments with MgONP as the adsorbent were conducted under identical conditions, and the maximum capacity was determined to be 156.4 mg/g. By plotting an absorbance plot, as shown in Figure 4, the band gap value for synthetic MgONP was determined to be 4.688 eV, which was lower than the band gap value for bulk MgO (7.8 eV), demonstrating the surface reactivity of synthesized MgONP.

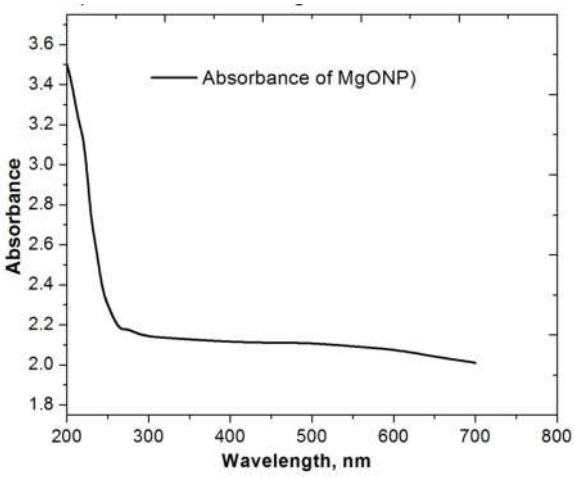

Figure 4. Absorbance plot for MgONP.

CONCLUSIONS

(1) The adsorption equilibrium agitation time for MgONP-AC was determined to be 60 min. The faster equilibrium might be attributed to magnesium oxide nanoparticles' positive surface charge throughout a wide pH range, which has a higher affinity for anionic dyes. (2) At the optimal variables of pH 7.68, dosage of 0.24 g/L, and MO concentration of 15 mg/L at 313 K, the MO elimination was determined to be 98.99% with CCD-RSM and 99.63% with ANN. (3) For the adsorbent, the kinetics data followed pseudo-second order kinetics and the isotherm data followed the Langmuir isotherm. (4) Positive enthalpy change (ΔH) values for both adsorbents suggested an endothermic and irreversible process. (5) FTIR research revealed that the stacking interaction between the aromatic backbone of the methyl orange dye and the skeleton of activated carbon leads to better adsorption. (6) The adsorption capacity, which is a key metric for determining the appropriateness of an adsorbent, was determined to be 345.91 mg/g for MgONP-AC.

REFERENCES

1. Ahmad, Z.U.; Yao, L.; Lian, Q.; Islam, F.; Zappi, M.E.; Gang, D.D. The use of artificial neural network (ANN) for modeling adsorption of sunset yellow onto neodymium modified ordered mesoporous carbon. *Chemosphere* **2020**, 256, 127081.
2. Saravanakumar, K.; Naveen Prasad, B.S.; Senthilkumar, R.; Reddy Prasad, D.M.; Venkatesan, D. Single and competitive sorption potential of date seed-derived biochar during removal of lead(II) and cadmium(II) ions. *Environ. Prog. Sustain. Energy.* **2021**, 40, 1-10.
3. Aravind Kumar, J.; Joshua Amarnath, D.; Anuradha Jabasingh, S.; Senthil Kumar, P.; Vijai Anand, K.; Narendrakumar, G.; Karthick Raja Namasivayam, S.; Krithiga, T.; Sunny, S.; Purna Pushkala, S.; Yuvarajan, D. One pot green synthesis of nano magnesium oxide-carbon composite: Preparation, characterization and application towards anthracene adsorption. *J. Clean. Prod.* **2019**, 237, 117691
4. Saravanakumar, K.; Senthilkumar, R.; Prasad, D.M.R.; Prasad, B.S.N.; Manickam, S.; Gajendiran, V. Batch and column arsenate sorption using turbinaria ornata seaweed derived biochar: Experimental studies and mathematical modeling. *ChemistrySelect* **2020**, 5, 3661–

3668.
5. Senthilkumar, R.; Reddy Prasad, D.M.; Govindarajan, L.; Saravanakumar, K.; Naveen Prasad, B.S. Improved sorption of reactive black 5 by date seed-derived biochar: isotherm, kinetic, and thermodynamic studies. *Sep. Sci. Technol.* **2019**, 54, 2351–2360.
6. Senthilkumar, R.; Reddy Prasad, D.M.; Govindarajan, L.; Saravanakumar, K.; Naveen Prasad, B.S. Synthesis of green marine algal-based biochar for remediation of arsenic(V) from contaminated waters in batch and column mode of operation. *Int. J. Phytoremediation* **2020**, 22, 279–286.
7. Azad, F.N.; Ghaedi, M.; Asfaram, A.; Jamshidi, A.; Hassani, G.; Goudarzi, A.; Azqhandi, M. H.A.; Ghaedi, A. Optimization of the process parameters for the adsorption of ternary dyes by Ni doped FeO(OH)-NWs–AC using response surface methodology and an artificial neural network. *RSC Adv.* **2016**, 6, 19768–19779.
8. Bagheri, A.R.; Ghaedi, M.; Asfaram, A.; Hajati, S.; Ghaedi, A.M.; Bazrafshan, A.; Rahimi, M.R. Modeling and optimization of simultaneous removal of ternary dyes onto copper sulfide nanoparticles loaded on activated carbon using second-derivative spectrophotometry. *J Taiwan Inst. Chem. Eng.* **2016**, 65, 212–224.
9. Khan, M.M.R.; Mukhlish, M.Z.B.; Mazumder, M.S.I.; Ferdous, K.; Prasad, D.M.R.; Hassan, Z. Uptake of indosol Dark-blue GL dye from aqueous solution by water hyacinth roots powder: Adsorption and desorption study. *Int. J. Environ. Sci. Technol*. **2014**, 11, 1027–1034.
10. Bhattacharya, P.; Swain, S.; Giri, L.; Neogi, S. Fabrication of magnesium oxide nanoparticles by solvent alteration and their bactericidal applications. *J Mater Chem B* **2019**, 7, 4141–4152.
11. Bhaviya Raj, R.; Umadevi, M.; Parimaladevi, R. Enhanced photocatalytic degradation of textile dyeing wastewater under UV and visible light using ZnO/MgO nanocomposites as a novel photocatalyst. *Part. Sci. Technol.* **2019**, 38, 1–9.
12. Cai, L.; Chen, J.; Liu, Z.; Wang, H.; Yang, H.; Ding, W. Magnesium oxide nanoparticles: Effective agricultural antibacterial agent against Ralstonia solanacearum. *Front. Microbiol.* **2018**, 9, 1–19.
13. Cao, C.Y.; Qu, J.; Wei, F.; Liu, H.; Song, W.G. Superb adsorption capacity and mechanism of flowerlike magnesium oxide nanostructures for lead and cadmium ions. *ACS Appl. Mater. Interfaces* **2012**, 4, 4283–4287.
14. Chaukura, N.; Murimba, E.C.; Gwenzi, W. Synthesis, characterisation and methyl orange adsorption capacity of ferric oxide–biochar nano-composites derived from pulp and paper sludge. *Appl. Water Sci.* **2016**, 7, 2175–2186.
15. Dayananda, D.; Sarva, V.R.; Prasad, S.V.; Arunachalam, J.; Parameswaran, P.; Ghosh, N.N. Synthesis of MgO nanoparticle loaded mesoporous Al2O3and its defluoridation study. *Appl. Surf. Sci.* **2015**, 329, 1–10.
16. Dhal, J.P.; Sethi, M.; Mishra, B.G.; Hota, G. MgO nanomaterials with different morphologies and their sorption capacity for removal of toxic dyes. *Mater. Lett.* **2015**, 141, 267–271.
17. Franco, D.S.P.; Duarte, F.A.; Salau, N.P.G.; Dotto, G.L. Analysis of indium(III) adsorption from leachates of LCD screens using artificial neural networks (ANN) and adaptive neuro-fuzzy inference systems (ANIFS). *J. Hazard Mater.* **2020**, 384, 121137.
18. Gadekar, M.R.; Ahammed, M.M. Modelling dye removal by adsorption onto water treatment residuals using combined response surface methodology-artificial neural network approach. *J. Environ. Manage.* **2019**, 231, 241–248.
19. Senthilkumar, R.; Reddy Prasad, D.M.; Lakshmanarao, G.; Krishnan, S.; Naveen Prasad, B.S. Ocean-based sorbents for decontamination of metal-bearing wastewaters: A review. *Environ. Technol. Rev.* **2018**, 7, 139–155.
20. Heidarizad, M.; Şengör, S.S. Synthesis of graphene oxide/magnesium oxide nanocomposites with high-rate adsorption of methylene blue. *J. Mol. Liq.* **2016**, 224, 607–617.
21. Hu, J.; Song, Z.; Chen, L.; Yang, H.; Li, J.; Richards, R. Adsorption properties of MgO(111) nanoplates for the dye pollutants from wastewater. *J. Chem. Eng. Data*, **2010**, 55, 3742–3748.

22. Imani, M.M.; Safaei, M. Optimized synthesis of magnesium oxide nanoparticles as bactericidal agents. *J. Nanotechnol.* **2019**, 2019, Article ID 6063832.
23. Jadhav, A.H.; Lim, A.C.; Thorat, G.M.; Jadhav, H.S.; Seo, J.G. Green solvent ionic liquids: Structural directing pioneers for microwave-assisted synthesis of controlled MgO nanostructures. *RSC Adv.* **2016**, 6, 31675–31686.
24. Jeevanandam, J.; Chan, Y.S.; Danquah, M.K. Biosynthesis and characterization of MgO nanoparticles from plant extracts via induced molecular nucleation. *New J. Chem.* **2017**, 41, 2800–2814.
25. Kulkarni, J.; Ravishankar, R.; Nagabhushana, H.; Anantharaju, K.S.; Basavaraj, R.B.; Sangeeta, M.; Nagaswarupa, H.P.; Renuka, L. Structural, optical and photocatalytic properties of MgO/CuO nanocomposite prepared by a solution combustion method. *Mater. Today: Proc.* **2017**, 4, 11756–11763.
26. León, G.; García, F.; Miguel, B.; Bayo, J. Equilibrium, kinetic and thermodynamic studies of methyl orange removal by adsorption onto granular activated carbon. *Desalination Water Treat.* **2016**, 57, 17104–17117.
27. Li, Y.Y.; Wan, M.M.; Lin, W.G.; Wang, Y.; Zhu, J.H. A novel porous MgO sorbent fabricated through carbon insertion. *J. Mater. Chem. A* **2014**, 2, 12014.
28. Liu, W.J.; Jiang, H.; Tian, K.; Ding, Y.W.; Yu, H.Q. Mesoporous carbon stabilized MgO nanoparticles synthesized by pyrolysis of $MgCl_2$ preloaded waste biomass for highly efficient CO_2 capture. *Environ. Sci. Technol.* **2013**, 47, 9397–9403.
29. Mahmoud, H.R.; Ibrahim, S.M.; El-Molla, S.A. Textile dye removal from aqueous solutions using cheap MgO nanomaterials: Adsorption kinetics, isotherm studies and thermodynamics. *Adv. Powder Technol.* **2016**, 27, 223–231.
30. Moradi Dehaghi, S.; Rahmanifar, B.; Moradi, A.M.; Azar, P.A. Removal of permethrin pesticide from water by chitosan-zinc oxide nanoparticles composite as an adsorbent. *J. Saudi Chem. Soc.* **2014**, 18, 348–355.
31. Moussavi, G.; Mahmoudi, M. Removal of azo and anthraquinone reactive dyes from industrial wastewaters using MgO nanoparticles. *J. Hazard. Mater.* **2009**, 168, 806–812.
32. Myneni, V.R.; Kanidarapu, N.R.; Vangalapati, M. Methylene blue adsorption by magnesium oxide nanoparticles immobilized with chitosan (CS-MgONP): Response surface methodology, isotherm, kinetics and thermodynamic studies. *Iran. J. Chem. Chem. Eng.* **2020**, 39, 29–42.
33. Myneni, V.R.; Punugoti, T.; Kala, N.S.; Kanidarapu, N.R.; Vangalapati, M. Modelling and optimization of methylene blue adsorption onto magnesium oxide nanoparticles loaded onto activated carbon (MgONP-AC): Response surface methodology and artificial neural networks. *Mater Today: Proc.* **2019**, 18, 4932–4941.
34. Nga, N.K.; Hong, P.T.T.; Lam, T.D.; Huy, T.Q. A facile synthesis of nanostructured magnesium oxide particles for enhanced adsorption performance in reactive blue 19 removal. *J. Colloid Interface Sci.* **2013**, 398, 210–216.
35. Niu, H.; Yang, Q.; Tang, K.; Xie, Y. Large-scale synthesis of single-crystalline MgO with bone-like nanostructures. *J. Nanoparticle Res.* **2006**, 8, 881–888.
36. Onu, C.E.; Nwabanne, J.T.; Ohale, P.E.; Asadu, C.O. Comparative analysis of RSM, ANN and ANFIS and the mechanistic modeling in eriochrome black-T dye adsorption using modified clay. *South Afr. J. Chem. Eng.* **2021**, 36, 24–42.
37. Pavan Kumar, G.V.S.R.; Malla, K.A.; Yerra, B.; Srinivasa Rao, K. Removal of Cu(II) using three low-cost adsorbents and prediction of adsorption using artificial neural networks. *Appl. Water Sci*. **2019**, 9, 1–9.
38. Purwajanti, S.; Zhang, H.; Huang, X.; Song, H.; Yang, Y.; Zhang, J.; Niu, Y.; Meka, A.K.; Noonan, O.; Yu, C. Mesoporous magnesium oxide hollow spheres as superior arsenite adsorbent: Synthesis and adsorption behavior. *ACS Appl. Mater. Interfaces* **2016**, 8, 25306–25312.

39. Rao, R.; Tanzi, M.; Tavakkoli, M.; Sahu, J.N. Optimization and modeling of methyl orange adsorption onto polyaniline nano-adsorbent through response surface methodology and diff erential evolution embedded neural network. *J. Environ. Manage.* **2018**, 223, 517–529.
40. Rojas-Mayorga, C.K.; Aguayo-Villarreal, I.A.; Moreno-Pérez, J.; Muñiz-Valencia, R.; Montes-Morán, M.Á.; Ocampo-Pérez, R. Influence of calcium species on SO2 adsorption capacity of a novel carbonaceous materials and their ANN modeling. *J. Environ. Chem. Eng.* **2021**, 9, 104810.
41. Sierra-Fernandez, A.; De La Rosa-García, S.C.; Gomez-Villalba, L.S.; Gómez-Cornelio, S.; Rabanal, M.E.; Fort, R.; Quintana, P. Synthesis, photocatalytic, and antifungal properties of MgO, ZnO and Zn/Mg oxide nanoparticles for the protection of calcareous stone heritage. *ACS Appl. Mater. Interfaces*. **2017**, 9, 24873–24886.
42. Siriwardane, I.W.; Udangawa, R.; de Silva, R.M.; Kumarasinghe, A.R.; Acres, R.G.; Hettiarachchi, A.; Amaratunga, G.A.J.; de Silva, K.M.N. Synthesis and characterization of nano magnesium oxide impregnated granular activated carbon composite for H_2S removal applications. *Mater. Des.* **2017**, 136, 127–136.
43. Tanhaei, B.; Ayati, A.; Iakovleva, E.; Sillanpää, M. Efficient carbon interlayed magnetic chitosan adsorbent for anionic dye removal : Synthesis , characterization and adsorption study. *Int. J. Biol. Macromol.* **2020**, 164, 3621–3631.
44. Tanhaei, B.; Ayati, A.; Lahtinen, M.; Sillanpää, M. Preparation and characterization of a novel chitosan/Al_2O_3/magnetite nanoparticles composite adsorbent for kinetic, thermodynamic and isotherm studies of Methyl Orange adsorption. *Chem. Eng. J.* **2015**, 259, 1–10.
45. Venkata Ratnam, M.; Karthikeyan, C.; Nagamalleswara Rao, K.; Meena, V. Magnesium oxide nanoparticles for effective photocatalytic degradation of methyl red dye in aqueous solutions: Optimization studies using response surface methodology. *Mater Today: Proc.* **2019**, 26, 2308–2313.